LIDAR SYSTEM CALIBRATION: IMPACT ON PLANE SEGMENTATION AND PHOTOGRAMMETRIC DATA REGISTRATION

Ayman Habib, Ki-In Bang, Ana Paula Kersting
Dept. of Geomatics Engineering, University of Calgary, 2500 University Dr. NW,
Calgary, Alberta, T2N 1N4, Canada.
ahabib@ucalgary.ca
kibang@ucalgary.ca
ana.kersting@ucalgary.ca

ABSTRACT

The availability of 3D surface data is crucial for several industrial, public, and military applications. Light Detection And Ranging (LiDAR) is an active sensor system capable of collecting 3D information from an object surface using laser pulses. Accurate and dense LiDAR data can be utilized for georeferencing of photogrammetric data and segmentation of 3D buildings. LiDAR data contaminated by systematic errors cannot guarantee the achievement of the expected accuracy and discrepancies might occur between overlapping strips. This paper presents an alternative method for LiDAR system calibration. In the proposed method, biases in LiDAR system parameters are estimated using time-tagged point cloud and trajectory data (position only). Unlike conventional calibration methods, the proposed method does not require raw measurements like GPS/INS observations, scan-mirror angles, and laser ranges for the laser footprints. The influence of LiDAR system calibration is analyzed through the evaluation of the relative and absolute accuracy before/after the calibration. Before calibration, segmentation procedure may produce unexpected planes because of positional errors of laser footprints and discrepancies between overlapping strips. For relative accuracy analysis, the plane segmentation result before the calibration will be compared to the planes segmented from re-constructed point cloud using the estimated biases in the system parameters. In addition, the impact of the LiDAR system calibration on the absolute accuracy of the point cloud is evaluated by using the LiDAR data for photogrammetric georeferencing before and after performing the proposed calibration procedure. Alternative primitives, such as straight lines extracted from the LiDAR point cloud are used as the control information. The absolute accuracy is evaluated through check point analysis when the photogrammetric reconstruction is done using the original/calibrated LiDAR features.

INTRODUCTION

LiDAR technology has been extensively used for the collection of a high density and high accurate topographic data. A LiDAR system is composed of a laser ranging and scanning unit and a position and orientation system (POS), which consists of an integrated differential global positioning system (DGPS) and an inertial measurement unit (IMU). The laser scanner measures distances from the sensor to the ground. The integrated GPS/IMU observations provide the position and attitude information of the scanner. The coordinates of the LiDAR points are the result of combining the derived measurements from each of its system components, as well as the mounting parameters relating such components. The relationship between the system measurements and parameters is embodied in the LiDAR equation (Vaughn et al., 1996; Schenk, 2001; El-Sheimy et al., 2005), Equation 1. As it can be seen in Figure 1, the position of the LiDAR point, $\bar{X}_G$, can be derived through the summation of three vectors ($\bar{X}_o$, $\bar{P}_G$ and $\bar{\rho}$) after applying the appropriate rotations: $R_{yaw,\ pitch,\ roll}$, $R_{\Delta\omega,\Delta\phi,\Delta\kappa}$ and $R_{\alpha,\ \beta}$. In this equation, $\bar{X}_o$ is the vector from the origin of the ground reference frame to the origin of the IMU coordinate system, $\bar{P}_G$ is the offset between the laser unit and IMU coordinate systems (lever-arm offset vector), and $\bar{\rho}$ is the laser range vector whose magnitude is equivalent to the distance from the laser firing point to its footprint. It should be noted that $\bar{X}_o$ is derived through the GPS/INS integration process while considering the lever-arm offset vector between the IMU body frame and the phase centre of the GPS antenna. The term $R_{yaw,\ pitch,\ roll}$ stands for the rotation matrix relating the ground and IMU coordinate systems – which is derived

through the GPS/INS integration process, $R_{\Delta\omega,\Delta\phi,\Delta\kappa}$ represents the rotation matrix relating the IMU and laser unit coordinate systems – which is defined by the bore-sighting angles, and $R_{\alpha,\beta}$ refers to the rotation matrix relating the laser unit and laser beam coordinate systems with α and β being the mirror scan angles. For a linear scanner, which is the focus of this research work, the mirror is rotated in one direction only, leading to zero α angle. The involved quantities in the LiDAR equation are all measured during the acquisition process except for the bore-sighting angles and lever-arm offset vector (mounting parameters), which are usually determined through a calibration procedure.

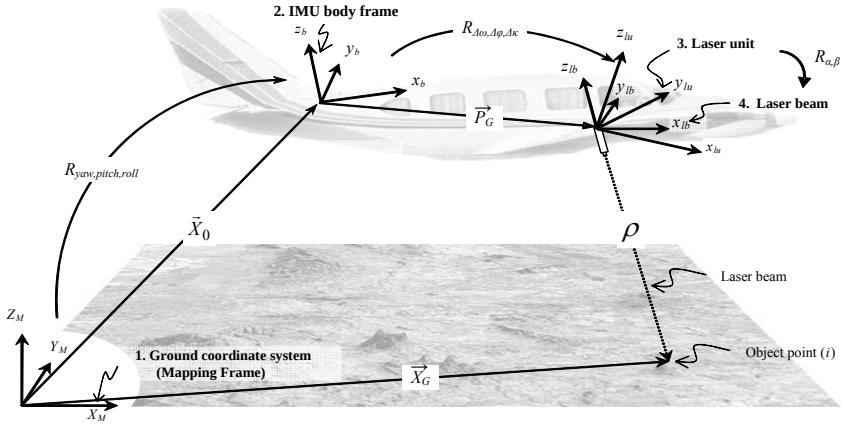

Figure 1. Coordinate systems and involved quantities in the LiDAR equation.

$$\vec{X}_G = \vec{X}_o + R_{yaw,\ pitch,\ roll}\ \vec{P}_G + R_{yaw,\ pitch,\ roll}\ R_{\Delta\omega,\ \Delta\varphi,\ \Delta\kappa}\ R_{S_\alpha\alpha,\,S_\beta\beta}\begin{bmatrix} 0 \\ 0 \\ -(\Delta\rho+\rho) \end{bmatrix} \qquad (1)$$

Due to systematic errors in the LiDAR components and/or resulting from their integration, adjacent LiDAR strips might exhibit vertical and horizontal discrepancies. Such discrepancies are caused by missing or improperly employed calibration and operational procedures. The elimination and/or reduction of the effect of systematic errors in the system parameters have been the focus of LiDAR research in the past few years. The existing approaches can be classified into two main categories: system driven (calibration) and data driven (strip adjustment) methods. System driven (or calibration) methods, which are considered by many researchers as the ideal solution (e.g., Filin, 2001; Morin, 2002; Skaloud and Lichti, 2006; Friess, 2006), are based on the physical sensor model relating the system measurements/parameters to the ground coordinates of the LiDAR points. These methods require the original observations (GPS/INS positions and attitudes, and the laser measurements) or at least the trajectory and time-tagged point cloud (Burman, 2000; Toth, 2002, Habib et al., 2010a), which might not be directly available to the end-user. Due to that fact, several approaches relying solely on the LiDAR point cloud coordinates, categorized as data-driven methods (or strip adjustment methods), have been proposed by several authors (Kilian et al., 1996; Crombaghs et al., 2000; Maas, 2002; Bretar et al., 2004; Filin and Vosselman, 2004; Pfeifer et al., 2005; Kager, 2004). In this approach, the effects of systematic errors are usually modeled by a straightforward transformation function between the laser strip coordinate system and a reference coordinate system.

The objective of this paper is to investigate the impact of the calibration procedure on the relative and the absolute accuracy of the LiDAR point cloud. For that purpose, a calibration procedure (Habib et al., 2010a) that overcomes the limitation of existing calibration procedures in terms of requirement for raw observations is outlined and extended. This calibration procedure is denoted as "Quasi-Rigorous" since it is based on few reasonable assumptions. It requires time-tagged LiDAR point cloud and navigation data (trajectory position) only. With the widespread adoption of the LAS format and the easy access to trajectory data, the availability of the necessary information to conduct such calibration procedure is not a concern. In terms of the nature of the needed data, the utilized calibration procedure has the same requirement as some of the existing techniques (e.g., Burman, 2000 and Toth, 2002). However, it provides advantages in terms of the utilized primitives and required pre-processing. In contrast to the methods proposed in Burman (2000) and Skaloud and Litchi (2006), the unknown parameters do not change with the extent of the area or the number of primitives being utilized in the calibration procedure. Moreover, this method can be applied in any type of terrain coverage and it is relatively easy to implement. Therefore, it can be used in every flight mission if needed. Besides, it

requires minimal interaction from the user, which can be completely eliminated after minor extension of the suggested procedure.

The paper starts by briefly describing the utilized calibration procedure and its extension to handle biases in the range measurements and in the scan mirror angle as well as the utilization of control data. Then, the performance and impact of the calibration procedure on the relative and absolute accuracy of the LiDAR point cloud is evaluated through experimental results from real data. Finally, the paper presents some conclusions and recommendations for future work.

CALIBRATION PROCEDURE

The calibration method used in this work was introduced in Habib et. al. (2010a). In this method, biases in the system parameters are estimated while reducing discrepancies between conjugate surface elements in overlapping strips and control data, if available. In Habib et. al. (2010a) only LiDAR strips were used in the calibration procedure. In the current work, vertical control is also added in the calibration procedure and the mathematical model is extended to include range and scan mirror angle scale biases.

The mathematical derivation of the presented calibration method assumes that we are dealing with a linear scanner and that the LiDAR system unit is almost vertical, which is quite realistic for flight missions using a fixed wing platform. Such assumptions simplify the LiDAR geometric model as represented by Equation 1 to the form in Equation 2.

$$\begin{aligned}\vec{X}_G &\approx \vec{X}_o + \begin{bmatrix}\cos\kappa & -\sin\kappa & 0\\ \sin\kappa & \cos\kappa & 0\\ 0 & 0 & 1\end{bmatrix}\begin{bmatrix}\Delta X\\ \Delta Y\\ \Delta Z\end{bmatrix} + \begin{bmatrix}\cos\kappa & -\sin\kappa & 0\\ \sin\kappa & \cos\kappa & 0\\ 0 & 0 & 1\end{bmatrix}\begin{bmatrix}1 & -\Delta\kappa & \Delta\varphi\\ \Delta\kappa & 1 & -\Delta\omega\\ -\Delta\varphi & \Delta\omega & 1\end{bmatrix}\begin{bmatrix}-(\rho+\Delta\rho)\sin(S\ \beta)\\ 0\\ -(\rho+\Delta\rho)\cos(S\ \beta)\end{bmatrix} \\ &= \vec{X}_o + \begin{bmatrix}\cos\kappa & -\sin\kappa & 0\\ \sin\kappa & \cos\kappa & 0\\ 0 & 0 & 1\end{bmatrix}\begin{bmatrix}\Delta X\\ \Delta Y\\ \Delta Z\end{bmatrix} + \begin{bmatrix}\cos\kappa & -\sin\kappa & 0\\ \sin\kappa & \cos\kappa & 0\\ 0 & 0 & 1\end{bmatrix}\begin{bmatrix}1 & -\Delta\kappa & \Delta\varphi\\ \Delta\kappa & 1 & -\Delta\omega\\ -\Delta\varphi & \Delta\omega & 1\end{bmatrix}\begin{bmatrix}x\\ 0\\ z\end{bmatrix}\end{aligned} \qquad (2)$$

where,

- $\Delta X, \Delta Y, \Delta Z$ are the components of the lever-arm offset vector $\vec{P}_G$,
- z is the vertical coordinate of the laser point with respect to the laser unit coordinate system, and
- x is the lateral coordinate of the laser point with respect to the laser unit coordinate system, which is the lateral distance (with the appropriate sign) between the LiDAR point in question and the projection of the flight trajectory onto the ground.

The LiDAR point coordinates $\vec{X}_G$, as presented in Equation 2, is function of the system parameters $\vec{x}$ and measurements $\vec{l}$ (Equation 3), and represent the true point coordinates $\vec{X}_{True}$. In the presence of biases in the system parameters, the LiDAR point coordinates will become biased ($\vec{X}_{Biased}$) and will be function of the system parameters and measurements as well as biases in the system parameters ($\delta\vec{x}$), as expressed by Equation 4. In Habib et. al. (2010a), only biases in the system mounting parameters, i.e., biases in the lever-arm offset components ($\delta\Delta X, \delta\Delta Y, \delta\Delta Z$), biases in the bore-sighting angles ($\delta\Delta\omega, \delta\Delta\varphi, \delta\Delta\kappa$), were investigated. In the current work, we will also investigate the impact of biases in the measured ranges ($\delta\Delta\rho$), and constant scale bias in the scan mirror angle (δS) (Equation 4). Equation 4 can be linearized with respect to the system parameters using Taylor series expansion, producing the form in Equations 5 and 6, after ignoring second and higher order terms. The term $\partial f / \partial \vec{x}$ represents the partial derivatives with respect to the system parameters, while the term $\partial f / \partial \vec{x}\ \delta\vec{x}$ represents the impact of the system biases onto the derived point cloud coordinates ($\delta\vec{X}_G$).

$$\vec{X}_G = \vec{X}_{True} = f(\vec{x}, \vec{l}) \qquad (3)$$

where,

$\vec{x} = (\Delta X, \Delta Y, \Delta Z, \Delta\omega,\ \Delta\varphi,\ \Delta\kappa, \Delta\rho, S)$

$\vec{l} = \left(\vec{X}_O, \omega, \varphi, \kappa, \beta, \rho\right)$

$$\vec{X}_{Biased} = f(\vec{x} + \delta\vec{x}, \vec{l}) \qquad (4)$$

where,

$\delta\vec{x} = (\delta\Delta X, \delta\Delta Y, \delta\Delta Z, \delta\Delta\omega,\ \delta\Delta\varphi,\ \delta\Delta\kappa, \delta\Delta\rho, \delta S)$

$$\vec{X}_{Biased} \approx f(\vec{x}, \vec{l}) + \frac{\partial f}{\partial \vec{x}}\delta\vec{x} = \vec{X}_{True} + \begin{bmatrix} \delta X_G \\ \delta Y_G \\ \delta Z_G \end{bmatrix} \qquad (5)$$

$$\vec{X}_{Biased} \approx \vec{X}_{True} + \begin{bmatrix} \delta X_G \\ \delta Y_G \\ \delta Z_G \end{bmatrix}_{\delta\Delta X,\ \delta\Delta Y,\ \delta\Delta Z} + \begin{bmatrix} \delta X_G \\ \delta Y_G \\ \delta Z_G \end{bmatrix}_{\delta\Delta\omega,\ \delta\Delta\varphi,\ \delta\Delta\kappa} + \begin{bmatrix} \delta X_G \\ \delta Y_G \\ \delta Z_G \end{bmatrix}_{\delta\Delta\rho,\ \delta S} = \vec{X}_{True} + \begin{bmatrix} \delta X_G \\ \delta Y_G \\ \delta Z_G \end{bmatrix}_{Total} \qquad (6)$$

The mathematical relationship between conjugate points in overlapping strips can be derived by rewriting Equation 6 for two overlapping strips (*A* and *B*) and subtracting the resulting equations from each other. Such a relationship is shown in Equation 7. Similarly, if control points are available, the mathematical relationship between control points and the LiDAR points can be derived by rewriting Equation 6 for the control surface (*A*) and the LiDAR strip (*B*) and subtracting the resulting equations from each other. Since the term $\partial f / \partial \vec{x}\ \delta\vec{x}$ will be equal to zero for the control surface, their mathematical relationship will be reduced to the form in Equation 8. It is important to mention that Equation 8 will be written for all LiDAR strips which overlap with the control surface.

Equations 7 and 8 are the final linear observation equations, when dealing with overlapping strips and control surfaces, respectively. These equations allow us to recover the biases in the system parameters $(\delta\Delta X, \delta\Delta Y, \delta\Delta Z, \delta\Delta\omega, \delta\Delta\phi, \delta\Delta\kappa, \delta\Delta\rho, \delta S)$ if trajectory position and time-tagged point cloud are available. It should be noted that, when using only overlapping strips, the vertical bias in the lever-arm offset parameters $(\delta\Delta Z)$ cannot be detected. Such inability is caused by the fact that a vertical bias in the lever-arm offset parameters produces the same effect regardless of the flying direction, flying height, or scan angle. When control data over flat horizontal surface (i.e., vertical control) is also employed, we cannot recover $\delta\Delta Z$ and $\delta\Delta\rho$ simultaneously due to the high correlation between these parameters. As can be observed in the third line in Equation 8, the vertical lever-arm offset bias ($-\delta\Delta Z$) and the range bias ($\cos(S\beta)\delta\Delta\rho$) are highly correlated in the range of the utilized scan angle (i.e., $\cos(S\beta) \approx 1$). Vertical control data will only contribute for the estimation of the roll $(\delta\Delta\phi)$ and the mirror angle scale biases (δS). The use of control data over sloped surfaces will contribute for the estimation of all parameters and might help decoupling $\delta\Delta Z$ and $\delta\Delta\rho$.

A detailed analysis of the impact of biases in the system parameters on the derived LiDAR point cloud in terms of flying direction, flying height, and scan angle dependency is presented in Habib et al., 2009a. In this work, the flight configuration that maximizes the impact and decouples systematic errors in the mounting parameters is investigated. It was mathematically demonstrated that working with four strips which are captured from two flying heights in opposite directions with 100% overlap are optimal for the recovery of the planimetric lever-arm offset parameters as well as the bore-sighting pitch and roll biases. In addition, two flight lines, which are flown in the same direction with the least overlap possible, are optimal for the recovery of the bore-sighting yaw and roll biases, range bias, and mirror angle scale bias.

Once the biases are recovered, we can reconstruct the corrected point cloud using Equation 9. In this equation, the terms $\left(\delta\hat{\Delta}X, \delta\hat{\Delta}Y, \delta\hat{\Delta}Z, \delta\hat{\Delta}\omega, \delta\hat{\Delta}\phi, \delta\hat{\Delta}\kappa, \delta\hat{\Delta}\rho, \delta\hat{S}\right)$ define the estimated biases in the system parameters.

$$\begin{bmatrix} X_A \\ Y_A \\ Z_A \end{bmatrix}_{Biased} - \begin{bmatrix} X_B \\ Y_B \\ Z_B \end{bmatrix}_{Biased} = \begin{bmatrix} (\cos\kappa_A - \cos\kappa_B)\delta\Delta X - (\sin\kappa_A - \sin\kappa_B)\delta\Delta Y \\ (\sin\kappa_A - \sin\kappa_B)\delta\Delta X + (\cos\kappa_A - \cos\kappa_B)\delta\Delta Y \\ 0 \end{bmatrix} +$$
$$+ \begin{bmatrix} (\sin\kappa_A z_A - \sin\kappa_B z_B)\delta\Delta\omega + (\cos\kappa_A z_A - \cos\kappa_B z_B)\delta\Delta\phi - (\sin\kappa_A x_A - \sin\kappa_B x_B)\delta\Delta\kappa \\ -(\cos\kappa_A z_A - \cos\kappa_B z_B)\delta\Delta\omega + (\sin\kappa_A z_A - \sin\kappa_B z_B)\delta\Delta\phi(\cos\kappa_A x_A - \cos\kappa_B x_B)\delta\Delta\kappa \\ -(x_A - x_B)\delta\Delta\phi \end{bmatrix} + \quad (7)$$
$$+ \begin{bmatrix} -[\cos\kappa_A \sin(S\beta_A) - \cos\kappa_B \sin(S\beta_B)]\delta\Delta\rho + (\cos\kappa_A z_A \beta_A - \cos\kappa_B z_B \beta_B)\delta S \\ -[\sin\kappa_A \sin(S\beta_A) - \sin\kappa_B \sin(S\beta_B)]\delta\Delta\rho + (\sin\kappa_A z_A \beta_A - \sin\kappa_B z_B \beta_B)\delta S \\ -[\cos(S\beta_A) - \cos(S\beta_B)]\delta\Delta\rho - (x_A \beta_A - x_B \beta_B)\delta S \end{bmatrix}$$

$$\begin{bmatrix} X_A \\ Y_A \\ Z_A \end{bmatrix}_{Control\ Surface} - \begin{bmatrix} X_B \\ Y_B \\ Z_B \end{bmatrix}_{Biased} = \begin{bmatrix} -\cos\kappa_B\ \delta\Delta X + \sin\kappa_B\ \delta\Delta Y \\ -\sin\kappa_B\ \delta\Delta X - \cos\kappa_B\ \delta\Delta Y \\ -\delta\Delta Z \end{bmatrix} +$$
$$+ \begin{bmatrix} -\sin\kappa_B z_B\ \delta\Delta\omega - \cos\kappa_B z_B\ \delta\Delta\phi + \sin\kappa_B x_B\ \delta\Delta\kappa \\ \cos\kappa_B z_B\ \delta\Delta\omega - \sin\kappa_B z_B\ \delta\Delta\phi - \cos\kappa_B x_B\ \delta\Delta\kappa \\ x_B\ \delta\Delta\phi \end{bmatrix} + \quad (8)$$
$$+ \begin{bmatrix} \cos\kappa_B \sin(S\beta_B)\delta\Delta\rho - \cos\kappa_B z_B \beta_B\ \delta S \\ \sin\kappa_B \sin(S\beta_B)\delta\Delta\rho - \sin\kappa_B z_B \beta_B\ \delta S \\ \cos(S\beta_B)\delta\Delta\rho + x_B \beta_B\ \delta S \end{bmatrix}$$

$$\begin{bmatrix} X \\ Y \\ Z \end{bmatrix}_{Corrected} = \begin{bmatrix} X \\ Y \\ Z \end{bmatrix}_{Biased} - \begin{bmatrix} \cos\kappa\,\delta\hat{\Delta}X - \sin\kappa\,\delta\hat{\Delta}Y + \sin\kappa z\,\delta\hat{\Delta}\omega + \cos\kappa z\,\delta\hat{\Delta}\phi \\ \sin\kappa\,\delta\hat{\Delta}X + \cos\kappa\,\delta\hat{\Delta}Y - c\cos\kappa z\,\delta\hat{\Delta}\omega + \sin\kappa z\,\delta\hat{\Delta}\phi \\ \delta\hat{\Delta}Z - x\,\delta\hat{\Delta}\phi \end{bmatrix} - \quad (9)$$
$$- \begin{bmatrix} -\sin\kappa x\,\delta\hat{\Delta}\kappa - \cos\kappa\sin(S\beta)\,\delta\Delta\hat{\rho} + c\cos\kappa z\,\beta\,\delta\hat{S} \\ \cos\kappa x\,\delta\hat{\Delta}\kappa - \sin\kappa\sin(S\beta)\,\delta\Delta\hat{\rho} + s\sin\kappa z\,\beta\,\delta\hat{S} \\ -\cos(S\beta)\,\delta\hat{\Delta}\rho - x\,\beta\,\delta\hat{S} \end{bmatrix}$$

The procedure for estimating the necessary quantities $(x, z, \text{and } k)$ presented in Equations 7 and 8 using the available data (time-tagged point cloud and trajectory positions), is as follows:

I. For a LiDAR point mapped at time (*t*), we search in the trajectory file for positions within a certain time interval ($t - \Delta t$, $t + \Delta t$);

II. Then, a straight line is fitted through the selected trajectory positions to come up with a local estimate of the trajectory. After defining the local trajectory, the necessary quantities can be estimated as follows:
   - *x,* which is the lateral coordinate of the laser point with respect to the laser unit coordinate system, can be determined by computing the normal distance (with the appropriate sign) between the LiDAR point and the interpolated trajectory data. The intersection of the normal from the LiDAR point to the interpolated trajectory will define the position of the trajectory at time *t*;
   - *z,* which is the vertical coordinate of the laser point with respect to the laser unit coordinate system, can be determined by subtracting the elevation of the laser firing point (*H*) at time *t*, given by the interpolated flight trajectory, from the LiDAR point elevation (*Z*), i.e., $z = Z - H$; and
   - κ, which is the trajectory heading, can be computed once we have the local estimate of the trajectory and its direction (defined by the neighbouring trajectory positions);

One should note that the established mathematical model for the calibration procedure is derived based on point primitives (i.e., conjugate points in overlapping strips). However, point-to-point correspondence in overlapping strips cannot be assumed due to the irregular nature of the LiDAR points. In this research, conjugate point and TIN

patch pairs are used as primitives and the Iterative Closest Patch (ICPatch) procedure is applied to establish their correspondence. When dealing with control information, the control data is represented by points and overlapping LiDAR strips by TIN patches. For more information regarding the ICPatch method, interested readers can refer to Habib et al., 2009a and Habib et al., 2010b. The utilization of conjugate point-patch pairs for the estimation of biases in the system parameters is accomplished through a weight modification for one of the points defining the TIN vertices (Habib et al., 2009b).

In summary, the Quasi-rigorous calibration procedure proceeds as follows:

(1) The correspondence between point-patch pairs is established using the Iterative Closest Patch (ICPatch) procedure;
(2) For each point-patch pair, one can write the observation equations similar to those in Equations 7 and 8, when dealing with overlapping strips and control surfaces, respectively;
(3) The initial correspondences are used to derive an updated estimate of the system biases. Then, the estimated system biases are used to reconstruct both surfaces using Equation 9. Since after reconstructing the LiDAR point cloud the correspondence between point-patch pairs might have changed, a new set of correspondences has to be established. The new correspondences are utilized to derive a better estimate of the system biases.
(4) Such a procedure is repeated until the corrections to the estimated calibration parameters are almost zero.

EVALUATION OF THE IMPACT OF THE CALIBRATION PROCEDURE

In this work, the impact of the proposed LiDAR system calibration procedure is analyzed through the evaluation of the relative and absolute accuracy of the LiDAR data before and after the calibration.

The impact on the relative accuracy will be evaluated by assessing the degree of compatibility between conjugate surface elements in overlapping strips before and after reconstructing the point cloud using the estimated system biases (Equation 9). Also, the impact of the calibration procedure on subsequent segmentation procedure will be investigated as well. The compatibility between conjugate surface elements in overlapping strips will be evaluated qualitatively and quantitatively. The qualitative evaluation will be performed by visual inspection of profiles generated using the original and adjusted point clouds to check any improvements in the quality of fit between overlapping strips. The quantitative assessment, on the other hand, will be performed by computing the 3D transformation parameters (discrepancies) between the overlapping strips before and after the calibration procedure. For the computation of the 3D transformation parameters, the ICPatch method will be employed. The implementation details of this method can be found in Habib et al., 2009a and Habib et al., 2010b.

To evaluate the impact of the calibration procedure on the absolute accuracy of the point cloud, LiDAR linear features, which are extracted from the original and adjusted point cloud, will be used for the georeferencing of an image block covering the same area. The methodology used for photogrammetric georeferencing utilizing control linear features is detailed in Shin et al., 2007. The absolute accuracy of the derived ground coordinates from the georeferenced image block is evaluated using a check point analysis.

EXPERIMENTAL RESULTS

Dataset Description

To evaluate the performance and test the validity of the proposed calibration methodology, a LiDAR dataset captured by a Leica ALS50, which complies with the optimum flight configuration, was utilized. The optimum flight configuration, as already discussed, consists of four strips which are captured from two flying heights in opposite directions with as much overlap as possible, and two flight lines, which are flown in the same direction with the least overlap possible. This configuration allows for the maximization of the impact of systematic biases and has the ability to decouple the different biases from each other. Figure 2 shows the characteristics of the acquired dataset and Table 1 presents the utilized overlapping strip pairs.

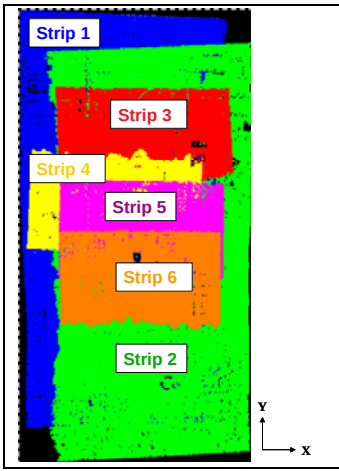

Strip Number	Flying Height	Direction
1	1150 m	N-S
2	1150 m	S-N
3	539 m	E-W
4	539 m	W-E
5	539 m	E-W
6	539 m	E-W

Figure 2. Configuration of the dataset (flying height and direction of the LiDAR strips).

Table 1. Overlapping strip pairs used in the calibration procedure

Overlapping Strips Cases	% of Overlap	Direction
Strips 1&2	80%	Opposite directions
Strips 3&4	25%	Opposite directions
Strips 4&5	75%	Opposite directions
Strips 5&6	50%	Same direction

Calibration Results

For the estimation of the biases in the system parameters besides the overlapping strip pairs described in Table 1, one vertical ground control point was used as well. The calibration results are presented in Table 2. Note that all system parameters biases are reported except the vertical bias in the lever-arm offset components $\delta\Delta Z$. Even though one vertical GCP was used, $\delta\Delta Z$ and $\delta\rho$ cannot be simultaneously recovered due to the high correlation between these parameters. In order to decouple $\delta\Delta Z$ and $\delta\rho$ vertical control data over sloped surfaces should be available. It can be noted in Table 2 that a significant bias in the bore-sighting roll angle was detected followed by a bias in the bore-sighting pitch angle.

Table 2. Estimated biases in the system parameters

$\delta\Delta X$ (m)	$\delta\Delta Y$ (m)	$\delta\Delta\omega$ (")	$\delta\Delta\phi$ (")	$\delta\Delta\kappa$ (")	$\delta\Delta\rho$ (m)	δS
-0.00	0.02	-39.6	-91.5	-7.45	0.07	0.0001589

Impact Analysis

The impact of the calibration procedure on the relative accuracy is assessed by checking the compatibility of the overlapping strips and evaluating the subsequent processing of the data (i.e., segmentation of the LiDAR point cloud) before and after the calibration procedure. The compatibility of the point cloud is evaluated qualitatively and quantitatively. The qualitative evaluation is performed by visual inspection of profiles generated using the original and adjusted point cloud to check any improvements in the quality of fit between overlapping strips. The improvement in the strips compatibility is illustrated in Figure 3, which shows a profile involving strips 1, 2, and 3 along the X direction, before and after the calibration procedure. The quantitative assessment, on the other hand, is performed by computing the discrepancies before and after the calibration procedure. The computed discrepancies are reported in Table 3. In this table, a significant improvement can be observed, especially in the across flight direction between strips flown in opposite directions (X_T direction for strips 1&2, and Y_T direction for strips 3&4 and strips 4&5 – refer to highlighted cells in Table 3). This is expected since a larger bias was estimated in the bore-

sighting roll angle, which mainly affects the across-flight direction (i.e., constant shift across the flight direction and a rotation around the flight direction). Insignificant improvement can be observed for strips 5&6 in Table 3. This is due to the fact that for strips flown in the same direction the roll bias only causes a constant vertical shift between conjugate surfaces elements with a much smaller magnitude. To evaluate the impact of the calibration on subsequent LiDAR processing, a segmentation technique was applied to the LiDAR dataset involving strips 1 and 2. For details about the segmentation technique employed, interested readers can refer to Kim and Habib (2009). It could be observed in the experiments that when segmenting large areas, i.e., using the same segmentation parameters for an area encompassing a variety of building types and sizes, the segmentation doesn't work for the whole area when using the data before the calibration procedure. More specifically, depending on the segmentation parameters selection, we might have planar patches not completely segmented (as illustrated in Figure 4a) or two different patches segmented as a single patch (e.g., adjacent patches with mild slope). After the calibration procedure, such problems don't take place as illustrated in the example given in Figure 4b. When segmenting smaller areas, such as the boxed area in Figure 5, and adjusting the segmentation parameters accordingly, we can get the segmentation results presented in Figure 6 before and after the calibration procedure. In this figure, improvements in the segmentation results after the calibration can be observed. However, they are not as significant as the improvement presented in Figure 4, since the segmentation parameters were changed to work properly with the data before the calibration. Regardless of having the planar patches correctly segmented, the profiles shown in Figure 5a and 5b show a significant reduction in the noise level of the LiDAR planar patches after the calibration procedure. The noise level reduction is also demonstrated in Table 3 which reports the average normal distance between the LiDAR points and the best fit plane through the points for the planar patches indicated in Figure 5, before and after the calibration procedure. As expected, larger improvement occurs for the planar patches with aspect parallel to the flight direction (patches 1 and 2) since the most significant detected bias was in the bore-sighting roll angle. Finally, Figure 7 shows the generated planar patch boundaries before and after the calibration on top of the aerial image. It can be observed that the generated boundaries after the calibration procedure are closer to the planar patch boundaries defined in the aerial image.

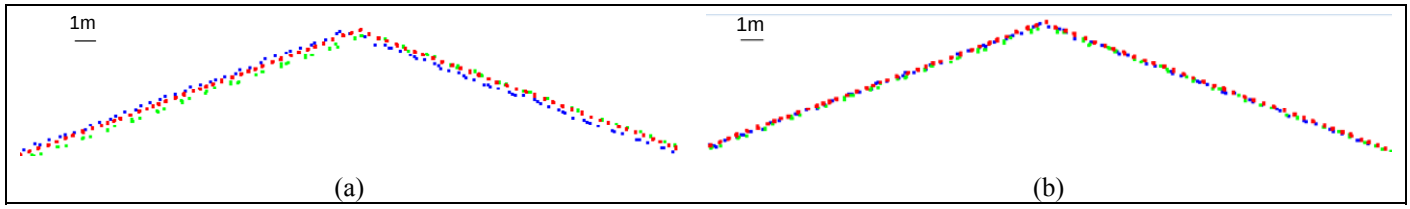

Figure 3. Profiles before (a) and after (b) the calibration procedure over a building covering strips 1, 2 and 3.

Table 3. Discrepancies between overlapping strips after applying the calibration parameters

Before Calibration			After Calibration		
Strips 1&2			Strips 1&2		
X_T (m)	Y_T (m)	Z_T(m)	X_T(m)	Y_T(m)	Z_T(m)
1.10	-0.32	-0.01	0.10	0.07	-0.05
ω (deg)	ϕ (deg)	κ (deg)	ω (deg)	ϕ (deg)	κ (deg)
0.0001	-0.052	-0.002	0.0012	-0.0016	-0.0055
Strips 3&4			Strips 3&4		
X_T (m)	Y_T (m)	Z_T(m)	X_T(m)	Y_T(m)	Z_T(m)
0.18	0.41	-0.01	-0.01	0.03	0.00
ω (deg)	ϕ (deg)	κ (deg)	ω (deg)	ϕ (deg)	κ (deg)
0.0484	-0.0005	-0.0011	0.0075	0.0009	-0.0013
Strips 4&5			Strips 4&5		
X_T (m)	Y_T (m)	Z_T(m)	X_T(m)	Y_T(m)	Z_T (m)
-0.13	-0.58	-0.12	0.05	-0.02	0.02
ω (deg)	ϕ (deg)	κ (deg)	ω (deg)	ϕ (deg)	κ (deg)
-0.0506	-0.0004	-0.0055	0.0069	-0.0007	-0.0030
Strips 5&6			Strips 5&6		
X_T (m)	Y_T (m)	Z_T (m)	X_T (m)	Y_T (m)	Z_T (m)
-0.06	-0.09	-0.08	-0.04	-0.01	0.02
ω (deg)	ϕ (deg)	κ (deg)	ω (deg)	ϕ (deg)	κ (deg)
-0.0049	0.0014	0.0068	0.0005	0.0017	0.0076

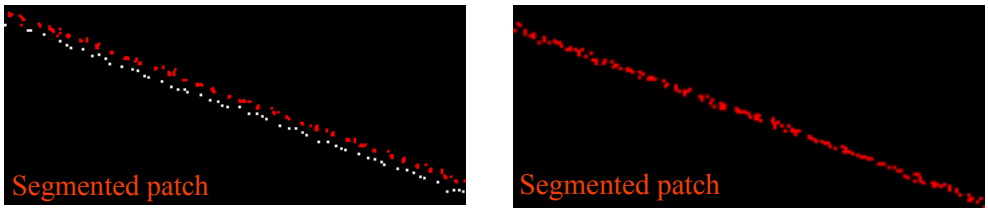

(a) (b)

Figure 4. LiDAR planar patch before the calibration procedure not completely segmented (a) LiDAR planar patch after the calibration procedure segmented correctly (b).

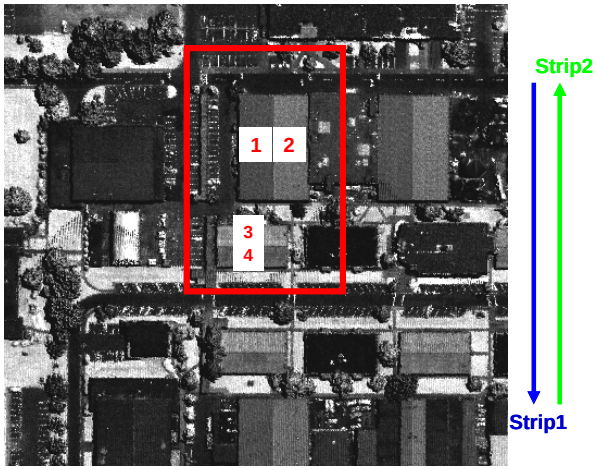

Figure 5. Segmented patches location.

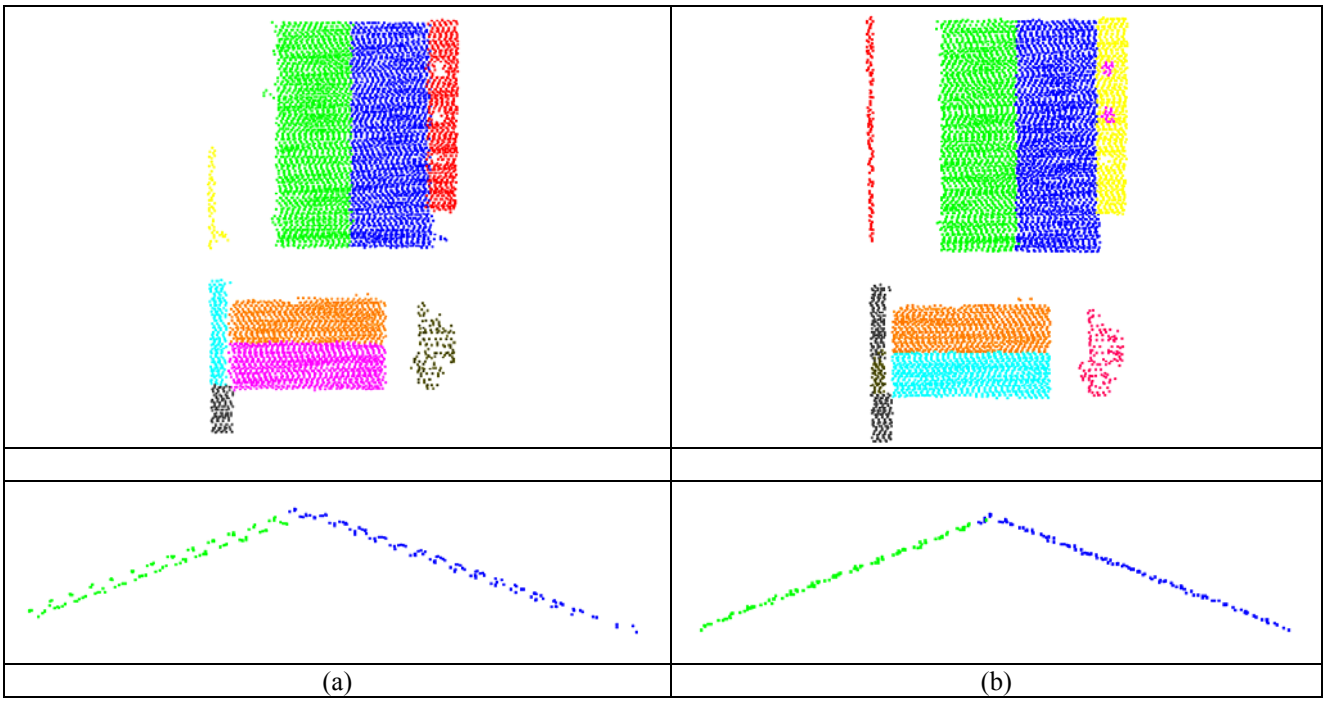

Figure 6. Segmentation results before (a) and after (b) the calibration procedure, utilizing an area covered by strips 1 and 2, as indicated in Figure 5.

Table 3. Noise level of the segmented LiDAR patches before and after the calibration procedure, utilizing an area covered by strips 1 and 2 (within the boxed area in Figure 5)

	Noise Level (m)	
	Before Calibration	**After Calibration**
Patch 1	0.23	0.06
Patch 2	0.16	0.06
Patch 3	0.10	0.04
Patch 4	0.05	0.05

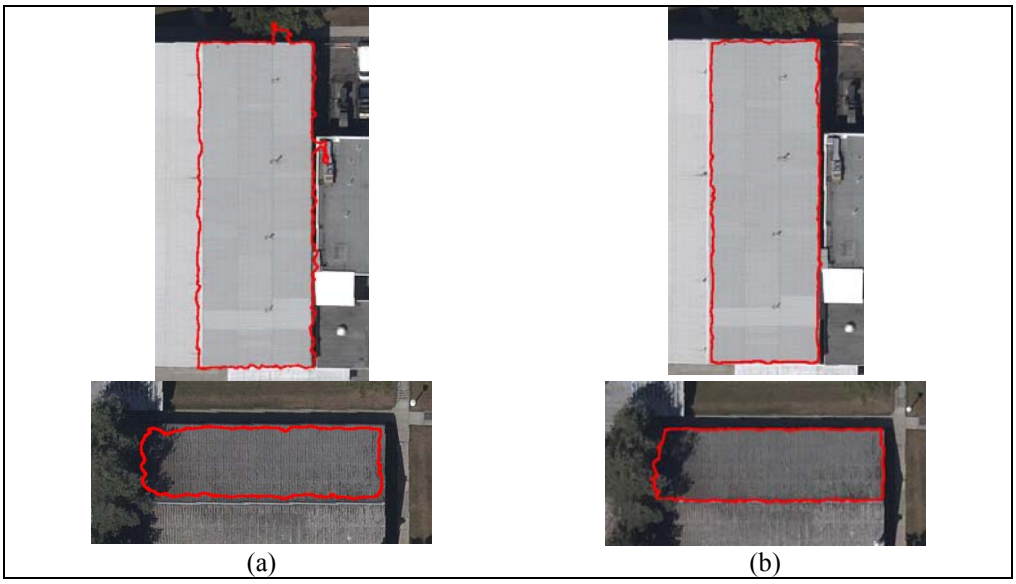

Figure 7. Boundary of a segmented planar patch before (a) and after (b) the calibration procedure.

To check the impact of the calibration procedure on the absolute accuracy, LiDAR linear features have been extracted and used for the georeferencing of an image block, which has been captured by a Rollei P-65 digital camera over the same area from two different flying heights (~550 and ~1200 m). The sensor ground sampling distance (GSD) is 5.50cm for a flying height of 550m and 12 cm for a flying height of 1200m. The utilized camera has an array dimension of 8984x6732 pixels and a focal length of 60 mm. The quality of the derived ground coordinates from the georeferenced image block was evaluated using a check point analysis. The results from the RMSE analysis for a total of 37 check points (GPS surveyed points) using the derived control linear features from the LiDAR point cloud before and after the calibration procedure are listed in Table 4. Significant improvement in the planimetric accuracy can be observed.

Table 4. RMSE analysis of the photogrammetric check points using extracted control linear features from the LiDAR data before and after the calibration procedure

	Before Calibration	*After Calibration*
Mean ΔX (m)	-0.03	0.02
Mean ΔY (m)	-0.18	0.01
Mean ΔZ (m)	0.15	0.08
σ_X (m)	0.11	0.05
σ_Y (m)	0.15	0.06
σ_Z (m)	0.17	0.18
$RMSE_X$ (m)	0.11	0.06
$RMSE_Y$ (m)	0.23	0.06
$RMSE_Z$ (m)	0.23	0.19
$RMSE_{TOTAL}$ (m)	0.34	0.21

Overall, the results of the impact of the calibration procedure on the relative and absolute accuracy are quite similar to the results presented in Habib et. al. (2010a). The additional modeled parameters and the used of control data haven't improved the results considerably. This can be explained by the fact that the main detected bias in the studied dataset is in the mounting parameters and mostly affect the horizontal accuracy.

CONCLUSIONS AND RECOMMENDATIONS FOR FUTURE WORK

In this paper, the impact of the system calibration on the relative and absolute LiDAR point cloud accuracy was evaluated. The calibration procedure introduced in Habib et. al., (2010a) was utilized and extended to handle biases in the range and in the scan mirror angle and control information. The calibration method employed is denoted as "Quasi-rigorous" since it is based on few reasonable assumptions. This method can deal with non-parallel strips and can handle heading variations and varying elevation heights since it makes use of time-tagged point cloud and trajectory position data.

The calibration procedure has been applied on a real dataset. The impact on the relative accuracy was evaluated by assessing the degree of compatibility between conjugate surface elements in overlapping strips before and after the system calibration. Also, the impact of the calibration procedure on subsequent segmentation was investigated as well. The compatibility between conjugate surface elements in overlapping strips was evaluated qualitatively and quantitatively. The qualitative evaluation of the calibration procedure was performed by visual inspection of profiles generated using the original and adjusted point cloud to check for any improvements in the quality of fit between overlapping strips. The quantitative evaluation, on the other hand, was performed by estimating the discrepancies between overlapping strips before and after reconstructing the LiDAR point cloud using the estimated biases in the system parameters. Qualitative and quantitative assessments have demonstrated a significant improvement in the quality of fit between overlapping strips – visually checked in profiles and in the computed discrepancies (e.g., the discrepancy between strips 1&2 across the flight direction was reduced from 1.10m to few centimetres). Also, it could be observed improvements in the outcome from the segmentation procedure (e.g., boundaries definition and noise level of the segmented planar patches). The impact on the absolute accuracy was assessed by using the LiDAR data for photogrammetric georeferencing before and after performing the proposed calibration procedure. The outcome of the photogrammetric reconstruction was evaluated through check point analysis. Significant improvement in the horizontal accuracy was demonstrated after removing the effect of estimated biases in the system parameters. For the studied dataset, the utilization of control data and the inclusion of the range and the scan mirror angle biases haven't considerably improved the results.

Future work will focus on extending the mathematical model to deal with non-linear scanners. In addition, effort will be placed towards the operability of the calibration procedures by automating the selection of the areas in the overlapping region as well as by improving the computational speed of the proposed methods (e.g. parallel processing). Moreover, more testing with real data from operational systems will be performed.

ACKNOWLEDGEMENT

This work was supported by the Canadian GEOIDE NCE Network (SII-72) and the National Science and Engineering Council of Canada (Discovery Grant). The authors would like to thank McElhanney Consulting Services Ltd, BC, Canada for providing the real LiDAR and image datasets. Also, the authors are indebted to Mr. Dan Tresa, McElhanney Consulting Services Ltd, for the valuable feedback.

REFERENCES

Bretar F., M. Pierrot-Deseilligny, and M. Roux, 2004. Solving the Strip Adjustment Problem of 3D Airborne Lidar Data, *Proceedings of the IEEE IGARSS'04,* 20-24 September, Anchorage, Alaska, 7, pp. 4734-4737.

Burman, H., 2000. *Calibration and Orientation of Airborne Image and Laser Scanner Data Using GPS and INS*, Ph.D. dissertation, Royal Institute of Technology, Stockholm. 125pages.

Crombaghs, M., E. De Min, and R. Bruegelmann, 2000. On the Adjustment of Overlapping Strips of Laser Altimeter Height Data, *International Archives of Photogrammetry and Remote Sensing*, 33(B3/1): 230-237.

El-Sheimy, N., C. Valeo, and A. Habib, 2005. *Digital Terrain Modeling: Acquisition, Manipulation And Applications,* Artech House Remote Sensing Library. 257 pages.

Friess, P., 2006. Toward a rigorous methodology for airborne laser mapping, *Proceedings EuroCOW*. 25-27

January, Castelldefels, Spain. 7 pages (on CD-ROM).

Filin, S., 2001. *Calibration of spaceborne and airborne laser altimeters using natural surfaces,* PhD Dissertation. Department of Civil and Environmental Engineering and Geodetic Science, the Ohio-State University, Columbus, OH. 129 pages.

Filin, S. and G. Vosselman, 2004. Adjustment of Airborne Laser Altimetry Strips, *The International Archives of the Photogrammetry, Remote Sensing and Spatial Information Sciences*, 35 (B3): 285-289.

Habib, A., K. Bang, A. P. Kersting, and D. C. Lee, 2009a. Error Budget of LiDAR Systems and Quality Control of the Derived Data, *Photogrammetric Engineering and Remote Sensing*, 75(9): 1093–1108.

Habib, A., A. P. Kersting, K. I. Bang, and M. Al-Durgham, 2009b. A Strip Adjustment Procedure to Mitigate the Impact of Inaccurate Mounting Parameters in Parallel LiDAR Strips, *The Photogrammetric Record*, 24(126): 171-195.

Habib, A., A. P. Kersting, and K. I. Bang, 2010a. Impact of LiDAR System Calibration on the Relative and Absolute Accuracy of the Adjusted Point Cloud, *EuroCOW Workshop on "Integrated Systems for Sensor Georeferencing and Navigation"*, Working Group 1/5, Spain.

Habib, A., A. P. Kersting, K. Bang, and D. C. Lee, 2010b. Alternative Methodologies for the Internal Quality Control of Parallel LiDAR Strips, *IEEE Transactions on Geoscience and Remote Sensing,* 48(1): 221-236.

Kager, H., 2004. Discrepancies Between Overlapping Laser Scanning Strips- Simultaneous Fitting of Aerial Laser Scanner Strips, *Proceedings of the International Society for Photogrammetry and Remote Sensing XXth Congress*, Istanbul, 34(B/1): 555 - 560.

Kilian, J., N. Haala, and M. Englich, 1996. Capture and evaluation of airborne laser scanner data, *International Archives of Photogrammetry and Remote Sensing*, 31(B3):383–388.

Kim, C. and A. Habib, 2009. Object-Based Integration of Photogrammetric and LiDAR Data for Automated Generation of Complex Polyhedral Building Models, *Sensors*, 9(7): 5679-5701

Maas H. G., 2002. Method for measuring height and planimetry discrepancies in airborne laserscanner data, *Photogrammetric Engineering and Remote Sensing*, 68(9): 933–940.

Morin, K.W., 2002. *Calibration of Airborne Laser Scanners*, M.S. thesis, University of Calgary, Department of Geomatics Engineering. 125 pages.

Pfeifer, N., S. O. Elberink, and S. Filin, 2005. Automatic Tie Elements Detection for Laser Scanner Strip Adjustment, *International Archives of Photogrammetry and Remote Sensing*, 36(3/W3): 1682-1750.

Schenk, T., 2001. Modeling and Analyzing Systematic Errors in Airborne Laser Scanners, *Technical Report in Photogrammetry* No. 19, Ohio Sate University. 42 pages.

Shin, S., Habib, A., Ghanma, M., Kim, C., and Kim, E., 2007. Algorithms for Multi-Sensor and Multi-Primitive Photogrammetric Triangulation, *ETRI Journal*, 29(4): 411-420.

Skaloud, J. and D. Lichti, 2006. Rigorous Approach to Bore-Sight Self-Calibration in Airborne Laser Scanning, *ISPRS Journal of Photogrammetry and Remote Sensing*, 61: 47–59.

Toth, C. K., 2002. Calibrating Airborne Lidar Systems. http://www.isprs.org/commission2/proceedings02/paper/084_100.pdf [Accessed: 15th November 2007].

Vaughn, C. R., J. L. Bufton, W. B. Krabill, and D. L. Rabine, 1996. Georeferencing of Airborne Laser Altimeter Measurements, *International Journal of Remote Sensing*, 17(11): 2185-2200.